Nonlocal cancellation of multi-frequency-channel dispersion

Xiaolong Hu, Tian Zhong, Franco N. C. Wong, Xiang Mao, Prashanta Kharel, Zhenda Xie, Xinan Xu, Chee Wei Wong, and Dirk R. Englund

Phys. Rev. A **91**, 013809 — Published 6 January 2015

DOI: 10.1103/PhysRevA.91.013809

Nonlocal Cancellation of Multi-Frequency-Channel Dispersion

Xiaolong Hu[1,2,3,*] Tian Zhong[2], Franco N. C. Wong[2], Xiang Mao[1],
Prashanta Kharel[1], Zhenda Xie[4], Xinan Xu[4], Chee Wei Wong[4], and Dirk R. Englund[2]
[1]*Department of Electrical Engineering, Columbia University, New York, NY 10027, USA*
[2]*Research Laboratory of Electronics, Massachusetts Institute of Technology, Cambridge, MA 02139, USA*
[3]*School of Precision Instrument and Opto-Electronic Engineering, Tianjin University, Tianjin 300072, China*
[4]*Department of Mechanical Engineering, Columbia University, New York, NY 10027, USA*
(Dated: December 8, 2014)

We present the first investigation of the temporal correlation of time-energy entangled photon pairs propagating through multi-frequency-channel dispersive media, in which photon spectra spread over multiple discrete frequency channels with dispersions. We have observed unique and more complex coincidence structures including double coincidence envelopes and dependence on frequency detuning that are absent in the single-channel case. Our results on the correlation of the time-energy photonic entanglement in dispersive media with channel divisions would impact the fields of quantum metrology and communication.

PACS numbers: 42.50.Ar, 42.65.Lm, 03.67.Hk

I. INTRODUCTION

Quantum interference can occur nonlocally. For example, Franson predicted [1] that when normal and anomalous dispersion are applied separately to the two photons of a time-energy entangled photon pair, the effect of dispersion can be remotely cancelled in their time correlation. Several interesting and inspiring experiments have been performed, including cancellations through nonlocal [2, 3] and local [4–6] interferences. Applications of dispersion cancellation range from quantum communication [7] and clock synchronization [8] to quantum-optical coherence tomography [9]. In particular, large-alphabet quantum key distribution (QKD) with dense wavelength division multiplexing (DWDM) was recently proposed [10] that would take advantage of the classical DWDM fiber-optic communication infrastructure. Classical DWDM systems use multiple frequency (wavelength) channels with pass bands that are slightly smaller than the channel spacing, and dispersive components for DWDM are designed to operate within each pass band. However, in quantum optics, the spectra of the correlated photons can spread over multiple discrete DWDM channels with dispersions. What would the photon correlation be after time-energy entangled photon pairs propagate through multi-frequency-channel dispersive media rather than continuously dispersive media that are typically assumed in previous quantum interference measurements [1–6]? Answering this question would be critically important for DWDM QKD systems in general for achieving photon-efficient, large-alphabet secure communications. However, such investigations, both theoretical and experimental, have not been reported.

We theoretically and experimentally investigate the effects of dispersion on time-energy entangled photons and its cancellation nonlocally in multi-frequency-channel dispersive media. The system studied here is presented in Fig. 1 (a). The difference between this system and the original one proposed by Franson [1] is that the dispersive components include discrete frequency channels and the spectra of signal and idler photons span over multiple frequency channels. For simplicity and as the first study, we use fiber-Bragg gratings, dispersive components commonly used in DWDM systems, which contain frequency channels each with the same frequency bandwidth and the same amount of group-velocity delay (GVD), as shown in Fig. 1(b). We observe the decrease of the temporal correlation, when normal or anomalous dispersion is applied only to signal or idler photons, and the recovery of the temporal correlation, when normal and anomalous dispersion are applied to signal and idler photons, respectively. We also observe unique and more complex coincidence structures including double coincidence envelopes and dependence on frequency detunings that are absent in the single-channel case. We discuss potential applications of this effect in sensitive spectroscopy and quantum communications.

Our paper is organized as follows: Sec. II presents the theory to model the temporal correlation of time-energy entangled photons propagating through multi-frequency-channel dispersive media. Sec. III shows the experimental investigation and the comparison between theoretical and experimental results. Sec. IV provides an intuitive, graphic explanation of the double coincidence envelope to further illustrate the physics of nonlocal cancellation of multi-frequency-channel dispersion. Sec. V concludes the paper.

II. THEORY

We first model the temporal correlation of time-energy entangled photons propagating through

* xiaolonghu@tju.edu.cn

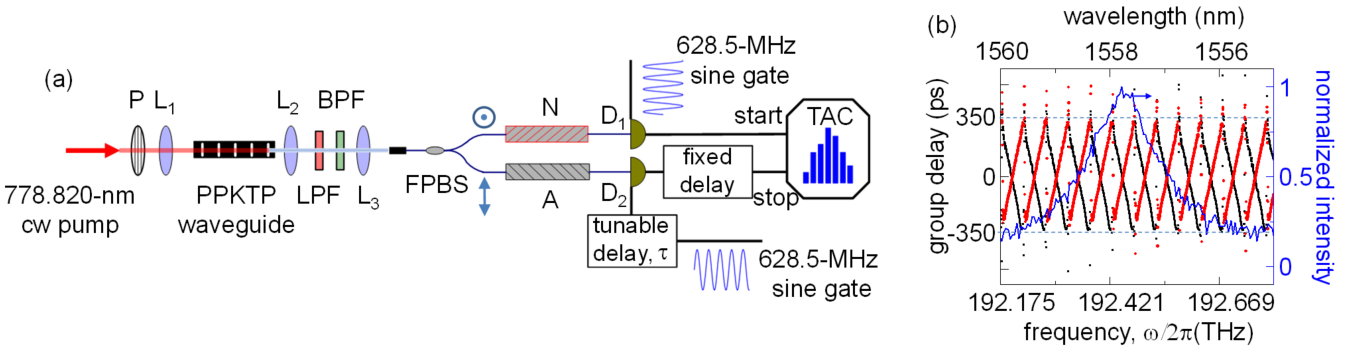

FIG. 1. (Color online) Experimental setup and dispersion for nonlocal cancellation of multi-frequency-channel dispersion. (a) Experimental setup: Time-energy entangled photon pairs are generated in a PPKTP waveguide, then coupled into and separated by a fiber polarization-beam splitter, after the pump photons are filtered out. Coincidence histogram is acquired after their propagation through dispersive media. cw: continuous wave; P: polarizer; L_1, L_2, L_3: lenses; PPKTP: periodically-poled potassium titanyl phosphate; LPF: long-pass filter; BPF: band-pass filter; FPBS: fiber polarization-beam splitter; τ: tunable electrical delay; TAC: time-to-amplitude converter. (b) Group-delay spectra of fiber Bragg gratings (FBGs) and the spectra of signal and idler photons. The channel width of FBGs is $2\sigma_g/2\pi = 48$ GHz and the maximum group delay is $T = 350$ ps and $-T = -350$ ps. Photon-pair spectra center at 1557.640 nm with a FWHM of 1.6 nm.

multi-frequency-channel dispersive media and predict what we would see in experiment. The joint detection probability of the detectors D_1 and D_2 between t_1 and $t_2 = t_1 + \tau$ is given by [1–3, 5] $P(\tau) = \left|\langle 0|E_2^+(x_2,t_2)E_1^+(x_1,t_1)|\Psi\rangle\right|^2$, where $E_i^+(x_i,t_i) = j\sum_{\omega_i}\left(\frac{2\pi\hbar\omega_i}{V}\right)^{1/2} e^{j[\phi_i(\omega_i)-\omega_i t_i]}$ is the positive frequency part of the electric field operator on detector D_i ($i = 1,2$); $j = \sqrt{-1}$; $|0\rangle$ is the vacuum state; $\phi_i(\omega_i)$ is an implicit function of x_i. $|\Psi\rangle = \int d\omega_1 d\omega_2 \rho(\omega_1,\omega_2) a^\dagger_{k_1}(\omega_1) a^\dagger_{k_2}(\omega_2)|0\rangle$ is the biphoton-state wavefunction. $\rho(\omega_1,\omega_2)$ is the joint biphoton spectrum. The list of symbols is also listed in Supplemental Material (SM) Section I. The biphoton state can be alternatively written as [1] $|\Psi\rangle \propto \int_0^{\omega_p} d\omega_1 f^2(\omega_1) a^\dagger_{k_1} a^\dagger_{k_p-k_1}|0\rangle$, where ($k_1$, ω_1), (k_2, ω_2), and (k_p, ω_p) characterize the modes of signal, idler, and pump photons, respectively. Frequency anti-correlation gives $\omega_1 = \omega_p/2 + \epsilon$ and $\omega_2 = \omega_p/2 - \epsilon$. We assume the Gaussian spectra as shown in Fig. 1 (b), $f(\omega_1) = e^{-(\omega_1-\omega_p/2)^2/2{\sigma_f}^2} = e^{-\epsilon^2/2{\sigma_f}^2}$. Therefore, the coincidence probability can be calculated by

$$P(\tau) \propto \left|\int_{-\infty}^{+\infty} d\epsilon e^{-\epsilon^2/{\sigma_f}^2 + j[\phi_1(\epsilon)+\phi_2(\epsilon)+\epsilon\tau]}\right|^2, \quad (1)$$

where ϕ_1 and ϕ_2 are the phases accumulated by propagating through dispersive media. The detailed derivation of Eq. (1) is shown in SM Section III.

Now we consider the phases, ϕ_1 and ϕ_2. In Fig. 1 (b) [also see Fig. S9 (b) in SM], the signal-idler spectra cover multiple frequency channels, which are labeled as $N = \cdots, -1, 0, 1, \cdots$. The channel containing $\omega_p/2$ is assigned to be $N = 0$ and the center of this channel is defined as ω_g. The width of each channel is $2\sigma_g$ and the maximum group delay is $\pm T$. The group delay can be analytically expressed as $\tau^N(\omega, N_N) = T/\sigma_g[\omega - (\omega_g + 2N_N\sigma_g)]$ and $\tau^A(\omega, N_A) = -T/\sigma_g[\omega - (\omega_g + 2N_A\sigma_g)]$, where N_N and N_A are the channel numbers of signal photons through the normal dispersive component and idler photons through the anomalous dispersive component, respectively. We further define δ as the detuning, $\delta = \omega_p/2 - \omega_g$, and s as the sign function of δ. Because of frequency anti-correlation, the following relations are valid for a particular pair of photons: $N_N + N_A = 0$, or, $N_N + N_A = s$. Because $\phi = -\int \tau(\omega)d\omega$, the phases due to propagation through dispersive media N and A are

$$\phi^N(\epsilon, N_N) = -\frac{T}{2\sigma_g}[\epsilon^2 \pm 2\epsilon(\delta - 2N_N\sigma_g)] + \phi_0^N, \quad (2)$$

and

$$\phi^A(\epsilon, N_A) = \frac{T}{2\sigma_g}[\epsilon^2 \pm 2\epsilon(\delta - 2N_A\sigma_g)] + \phi_0^A, \quad (3)$$

respectively. Eqs. (2) and (3) should use the plus (minus) sign if the corresponding dispersive component is placed in the stop (start) channel (SM Section IV).

We can explicitly write down (SM Sections V to VIII) the coincidence probability from Eqs. (1) - (3):

$$P(\tau) \propto \begin{cases} \left| \int_{-\infty}^{+\infty} \mathrm{d}\epsilon e^{-\frac{\epsilon^2}{{\sigma_\mathrm{f}}^2}+j\epsilon\tau} \right|^2, (4.1) \\ \left| \sum_{N=-\infty}^{+\infty} e^{-jN\omega_\mathrm{p}T} \int_{(2N-1)\sigma_\mathrm{g}-\delta}^{(2N+1)\sigma_\mathrm{g}-\delta} \mathrm{d}\epsilon e^{-\frac{\epsilon 2}{\sigma_\mathrm{f}^2}-j\frac{T}{2\sigma_\mathrm{g}}[\epsilon^2+2\epsilon(\delta-2N\sigma_\mathrm{g})]+j\epsilon\tau} \right|^2, (4.2) \\ \left| \sum_{N=-\infty}^{+\infty} e^{-jN\omega_\mathrm{p}T} \int_{(2N-1)\sigma_\mathrm{g}-\delta}^{(2N+1)\sigma_\mathrm{g}-\delta} \mathrm{d}\epsilon e^{-\frac{\epsilon^2}{\sigma_\mathrm{f}^2}+j\frac{T}{2\sigma_\mathrm{g}}[\epsilon^2+2\epsilon(\delta-2N\sigma_\mathrm{g})]+j\epsilon\tau} \right|^2, (4.3) \\ \left| \sum_{N=-\infty}^{+\infty} \int_{(2N-1)\sigma_\mathrm{g}+s\delta}^{(2N+1)\sigma_\mathrm{g}-s\delta} \mathrm{d}\epsilon e^{-\epsilon^2/\sigma_\mathrm{f}^2+j(\tau+2T\delta/\sigma_\mathrm{g})\epsilon} + \sum_{N=-\infty}^{+\infty} \int_{(2N-1)\sigma_\mathrm{g}-s\delta}^{(2N+1)\sigma_\mathrm{g}+s\delta} \mathrm{d}\epsilon e^{-\epsilon^2/\sigma_\mathrm{f}^2+j(\tau+2T\delta/\sigma_\mathrm{g})\epsilon-2sjT\epsilon} \right|^2, (4.4) \end{cases} \tag{4}$$

Eqs. (4.1), (4.2), (4.3), and (4.4) are coincidence probability with no dispersion, only normal dispersion, only anomalous dispersion, and both dispersion regimes, respectively. We define $R = e^{-{\tau^2}/{\sigma_\mathrm{J}}^2}$ as the instrument response function, in which σ_J is dominated by the timing jitter of the coincidence counting system. The coincidence probability, considering timing jitter, is the convolution of R and P: $P_\mathrm{J}(\tau) \propto R(\tau) \otimes P(\tau)$.

We can obtain the following insights about nonlocal cancellation of multi-frequency-channel dispersion by carefully examining Eq. (4). With no dispersive components along the path of photon-pair propagation, the coincidence probability, $P(\tau)$ in Eq. (4.1), is analytically integrable: $P(\tau) \propto \frac{{\sigma_\mathrm{f}}^2}{4\pi} e^{-\frac{\tau^2{\sigma_\mathrm{f}}^2}{2}}$, showing a Gaussian coincidence histogram with a full width at half maxima (FWHM) of $2^{\frac{3}{2}}\ln 2/\sigma_\mathrm{f}$ (SM Section V). Eqs. (4.2) and (4.3) represent the non-cancellation cases with one photon in the pair propagating through normal and anomalous dispersive components, respectively. Similar to Franson's original case without channel divisions [1], the $\pm j(T/2\sigma_\mathrm{g})\epsilon^2$ terms broaden the histogram; additionally, absent in Franson's case, a detuning (ϵ)- and channel (N)-dependent phase term, $j(T/2\sigma_\mathrm{g})2\epsilon(\delta - 2N\sigma_\mathrm{g})$, in each integral, complicates the coincidence structure. We solve this numerically for these two cases. What is particularly interesting is the dispersion-cancellation case in Eq. (4.4). Similar to Franson's case [1], the $\pm j(T/2\sigma_\mathrm{g})\epsilon^2$ terms are absent, showing the cancellation of GVD. In the case that $\sigma_\mathrm{g} \ll \sigma_\mathrm{f}$, i.e., the photon spectrum spans over many channels, $P(\tau)$ can be well approximated by (SM Section IX for the approximation and Section II for the definitions of various functions) $\mathrm{Gauss}^2(\tau + 2T\delta/\sigma_\mathrm{g}) \otimes [\mathrm{Sinc}^2(\tau + 2T\delta/\sigma_\mathrm{g}) \times \mathrm{Comb}(\tau + 2T\delta/\sigma_\mathrm{g})] + \mathrm{Gauss}^2(\tau + 2T\delta/\sigma_\mathrm{g} - 2sT) \otimes [{\mathrm{Sinc}_2}^2(\tau + 2T\delta/\sigma_\mathrm{g} - 2sT) \times \mathrm{Comb}_2(\tau + 2T\delta/\sigma_\mathrm{g} - 2sT)]$, which guide us towards the following predictions: (1) $P(\tau)$ is composed of two groups of Gaussian peaks, modulated by Sinc^2 functions, and the physical origin of the two groups, instead of one group or three or more, is due to the two time differences between correlated photons; (2) these two Sinc^2 functions center at $-2T\frac{\delta}{\sigma_\mathrm{g}}$ and $2T(s - \frac{\delta}{\sigma_\mathrm{g}})$; (3) the FWHM of the Gaussian peaks is $2^{\frac{3}{2}}\ln 2/\sigma_\mathrm{f}$, identical with the FWHM in the case without dispersive components; (4) the spacing between adjacent Gaussian peaks in each group is $\frac{\pi}{\sigma_\mathrm{g}}$; (5) the maximum of the first group of peaks, centered at $-2T\frac{\delta}{\sigma_\mathrm{g}}$, is proportional to $(\sigma_\mathrm{g} - |\delta|)^2$; the maximum of the second group of peaks, centered at $2T(s - \frac{\delta}{\sigma_\mathrm{g}})$, is proportional to δ^2; (6) the distance between two first zeros of the first sinc^2 function is $\frac{2\pi}{|\delta|}$, and therefore, the FWHM of this sinc^2 function is approximately $\frac{\pi}{|\delta|}$; the distance between two first zeros of the second sinc^2 function is $\frac{2\pi}{\sigma_\mathrm{g}-|\delta|}$, and therefore, the FWHM of this sinc^2 function is approximately $\frac{\pi}{\sigma_\mathrm{g}-|\delta|}$. Finally, carefully examining Eq. (4.4) leads to the following observation: (7) at special detuning $\delta = 0$, σ_g, and $-\sigma_\mathrm{g}$, Eq. (4.4) is identical to Eq. (4.1), representing a complete cancellation of both GVD and group-velocity mismatch. The sensitive dependence of the centers, maxima, and widths of the two envelopes on the detuning, δ, would be useful for sensing the shift of the biphoton spectrum, in applications such as spectroscopy and quantum communications. In what follows, we present our experimental observations.

III. EXPERIMENT

We measured the temporal correlation of time-energy entangled photons after propagation through multi-frequency-channel dispersive components, using the setup shown in Fig. 1 (a). Photon pairs were generated by pumping a 15-mm long periodically-poled potassium titanyl phosphate (PPKTP) waveguide (from AdvR) with a Ti:Sapphire tunable laser. The wavelength of the laser was initially tuned to be 778.820 nm ($\omega_\mathrm{p}/2\pi$ = 384.932 THz) and its linewidth was approximately 500 kHz. The temperature of the PPKTP was stabilized at 24.8 °C. Type-II quasi-phase-matching in the PPKTP waveguide

produced orthogonally polarized signal and idler photons, separable by a fiber polarizing beam splitter. The spectra of signal and idler photons were measured by a spatial grating and a CCD camera. The signal and idler photons were degenerate at the central wavelength of 1557.640 nm ($\omega_1/2\pi$ = 192.466 THz) with a full width at half maximum (FWHM) of 1.6 nm ($2\sqrt{\ln 2}\sigma_f/2\pi$ = 198 GHz) [13], as shown in Fig. 1 (d). Two fiber Bragg gratings (FBGs, from Teraxion) were used as multi-frequency-channel dispersive components. The channel widths for both FBGs were 0.4 nm ($2\sigma_g/2\pi$ = 48 GHz). The center of Channel 0 was at 1557.54 nm ($\omega_g/2\pi$ = 192.478 THz). The maximum positive and negative group delays, T and $-T$, in each channel, were 350 ps and -350 ps, respectively. The GVD in each channel, $\beta_2 L$, is therefore calculated to be ± 2321 ps^2. The spectra of group delay [12] are plotted in Fig. 1 (b). Temporal correlations were measured by coincidence counting using two self-differencing InGaAs/InP single-photon avalanche diodes (SPADs) [13] and a time-to-amplitude converter (HydraHarp 400 from PicoQuant). The SPADs were individually and sinusoidally gated at 628.5 MHz and their outputs were sent to start- and stop-channels of the HydraHarp with 4-ps timing resolution and <20-ps timing jitter for acquiring coincidence histograms. The two gate signals could be delayed relative to each other using an electronic phase shifter. At each gate delay, τ, coincidence counts were recorded and accidental counts were then subtracted.

We first measured the temporal correlations of the photon pairs at one detuning, $\delta/2\pi = 0.5\sigma_g/2\pi$ = 12 GHz. In Fig. 2, open squares are experimental data; error bars are one standard deviation according to Poissonian statistics of the photon pairs. Fig. 2 also present the numerical results of $P(\tau)$ and $P_J(\tau)$ in blue-dashed and red-solid lines, respectively. In Fig. 2 (a), without dispersive components, the measured photon correlation shows a FWHM of 353 ps through Gaussian fitting; the broadening was dominated by the instrument response time of the coincidence counting system. Thus, we approximated σ_J to be $353/(2\sqrt{\ln 2})$ ps. In Fig. 2 (b) and (c), with only normal or only anomalous dispersion, Gaussian fittings to the data show FWHMs of 623 ps and 659 ps, respectively, indicating the decrease of correlations. We found by numerical simulation that in these two cases with only normal or anomalous dispersion, the width of P_J is almost independent of the detuning, δ, in our studied regime $\sigma_f \gg \sigma_g$. In Fig. 2 (d), with both dispersions, the data clearly shows double peaks, corresponding to the two sinc^2 envelopes with broadening by $R(\tau)$. The data show the widths of 370 ps (left) and 361 ps (right) for these two peaks. Although numerically similar to the original width in Fig. 2 (a), these widths in Fig. 2 (d) are the result of combined effects of the cancellation of GVD and the channel division of the dispersive components. This double-peak feature in the

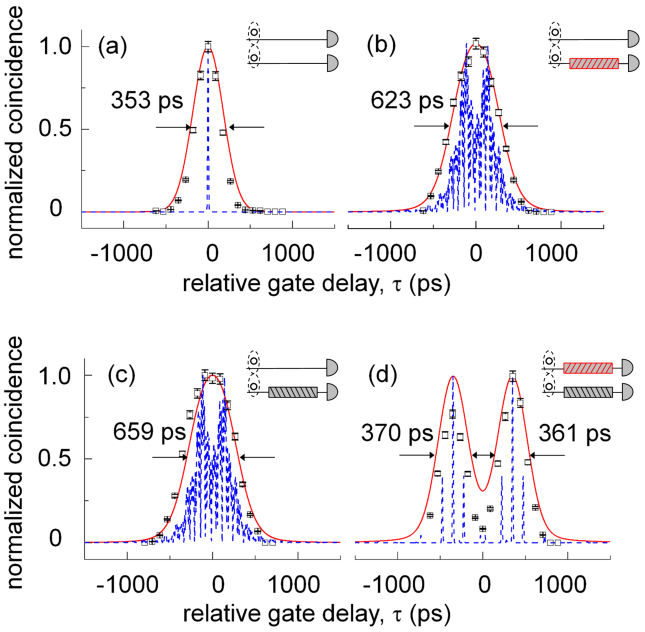

FIG. 2. (Color online) Temporal correlations of time-energy entangled photon pairs with (a) no dispersion; (b) signal photons propagating through no dispersion and idler photons propagating through normal dispersion; (c) signal photons propagating through no dispersion and idler photons propagating through anomalous dispersion; (d) signal and idler photons propagating through normal and anomalous dispersions, respectively. The insets show the configurations. Detuning: $\delta/2\pi = 0.5\sigma_g/2\pi$ = 12 GHz. Open squares: experimental data; error bars: one standard deviation according to Poissonian statistics of the photon pairs; blue-dashed lines: $P(\tau)$; red-solid lines: $P_J(\tau)$. Both experimental and numerical data are normalized to their maxima in each data set.

temporal correlation is dramatically different from what was predicted [1] and observed [2] previously, without channel divisions. Our theoretical results, $P_J(\tau)$ match the experimental data. Limited by the timing resolution of the SPADs, we unfortunately could not resolve the individual Gaussian peaks, as shown in blue-dashed lines, in each envelope. These Gaussian peaks with spacings of $\frac{\pi}{\sigma_g}$ = 21 ps might be barely resolvable by superconducting-nanowire single-photon detectors [14] with sub 30-ps timing jitter [15]. Using dispersive components with smaller σ_g would relax the stringent requirement for the timing resolution of the single-photon detectors.

We then investigated temporal correlations after GVD cancellation at different detuning, δ. Because of the periodic nature of dispersion of the FBGs used, the correlation histogram with a detuning of δ is equivalent to and theoretically identical to the correlation histogram with a detuning of $\delta - 2N\sigma_g$. We therefore tuned the pump wavelength so that the signal-idler spectra swept over one period, from

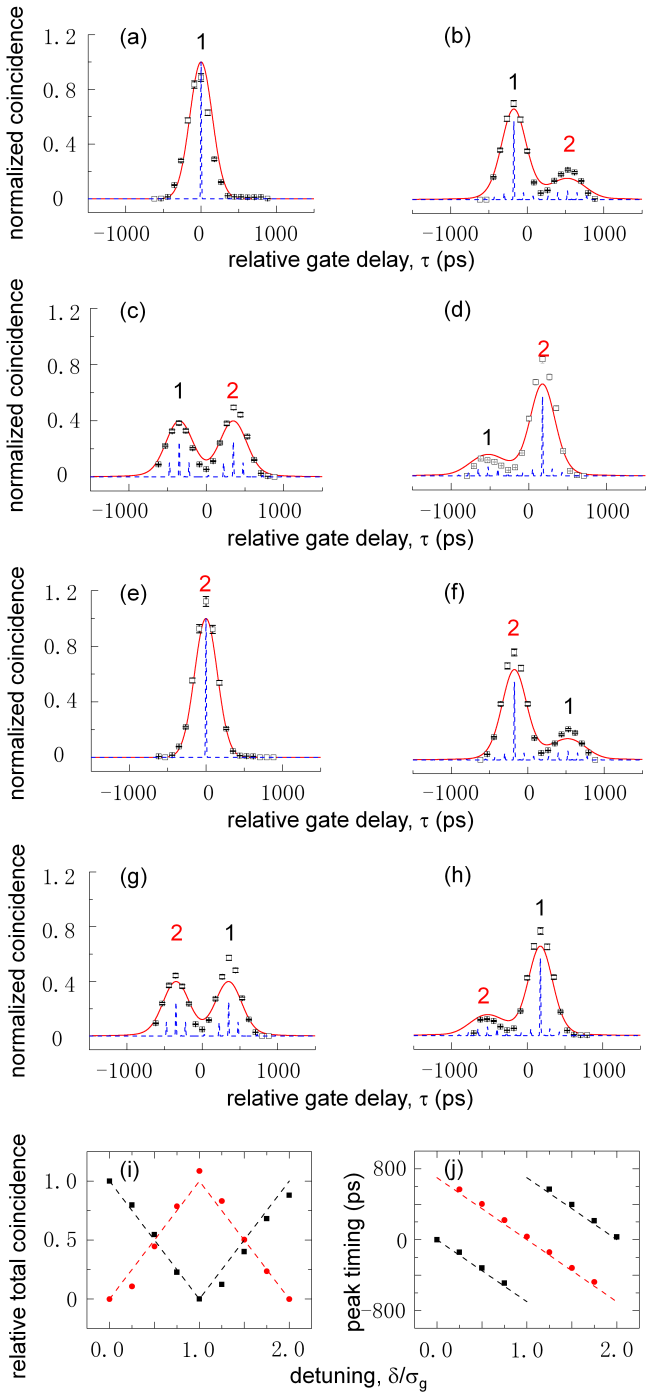

FIG. 3. (Color online) Temporal correlations with cancellation of multi-frequency-channel dispersion at detunings of (a) $\delta = 0$, (b) $\delta = 0.25\sigma_g$, (c) $\delta = 0.5\sigma_g$, (d) $\delta = 0.75\sigma_g$, (e) $\delta = \sigma_g$, (f) $\delta = 1.25\sigma_g$, (g) $\delta = 1.5\sigma_g$, and (h) $\delta = 1.75\sigma_g$. Open squares: experimental data; error bars: one standard deviation according to Poissonian statistics of the photon pairs; blue-dashed lines: $P(\tau)$; red-solid lines: $P_J(\tau)$. Experimental and numerical data are normalized to the maxima of their counterparts in (a). Two observed peaks are labeled as 1 and 2. (i) Relative total coincidence [normalized to the total coincidence in case (a)] in each peak obtained through fitting. (j) Peak timing obtained through fitting. Black squares: Peak 1; red dots: Peak 2; dashed lines: theoretical results.

1557.54 nm ($\omega_g/2\pi = 192.478$ THz) to 1557.34 nm [$(\omega_g + 2\sigma_g)/2\pi = 192.503$ THz], with a step size of -0.05 nm (3.1 GHz). Our calculation based on the phase-matching condition of the current waveguide spontaneous-parametric-down-conversion source shows that changing the pump wavelength from the degenerate pumping wavelength by 0.2 nm would yield a 0.02-nm (5% of the channel width) non-degeneracy of signal and idler photons; thus, we assume their degeneracy throughout our theoretical modeling. Fig. 3 (a) - (h) show the evolution of the observed double peaks at different detunings, δ. Experimental and numerical data are normalized to the maxima of their counterparts in Fig. 3 (a). The coincidence counts included in envelopes 1 and 2 change in a complementary way and the total coincidences are kept constant. The timing of the two envelopes both moves towards the $-\tau$ direction with increasing δ, with the time difference between these two envelopes kept constant: $2T = 700$ ps. At special detunings, $\delta = 0$ and $\delta = \sigma_g$, we only observed one peak and the other peak diminished, representing complete nonlocal dispersion cancellation of not only GVD but also the group-delay mismatch. These observations are all summarized in Fig. 3 (i) and (j), showing the relative total number of coincidence included in each peak and the timing of the peaks, respectively. The experimental results quantitatively agree with the theory.

IV. A GRAPHIC EXPLANATION OF THE DOUBLE OR SINGLE COINCIDENCE ENVELOPES RESULTING FROM NONLOCAL CANCELLATION OF MULTI-FREQUENCY-CHANNEL DISPERSION

To further illustrate the physics of nonlocal cancellation of multi-frequency-channel dispersion, we provide an intuitive, graphic explanation of the double envelopes at general detunings ($\delta \neq 0$ and $\delta \neq \sigma_g$) or the single peak at special detunings ($\delta = 0$ and $\delta = \sigma_g$) in the coincidence histogram that we have predicted and observed. The origin of the two groups of peaks at general detunings ($\delta \neq 0$ and $\delta \neq \sigma_g$), with one centered at $-2T\frac{\delta}{\sigma_g}$ and another at $2T(s - \frac{\delta}{\sigma_g})$, is the two time differences between signal and idler photons. Because of frequency anti-correlation, the two photons in one pair are always symmetrically located on the biphoton spectrum. Therefore, these two photons are either (1) in the channels satisfying $N_N + N_A = 0$ or (2) in the channels satisfying $N_N + N_A = s$, as discussed in Sec. II. As shown in Fig. 4(a), the spectral regions with open and filled circles represent the case (1) and (2), respectively. Careful examination [Fig. 4(b)] of the time difference between the two photons in one pair, resulting from the group-delay differences of the dispersive components, shows that in case (1), the time difference is ΔT_1; and in case (2), the time difference is ΔT_2. These two group-delay differences yield the two

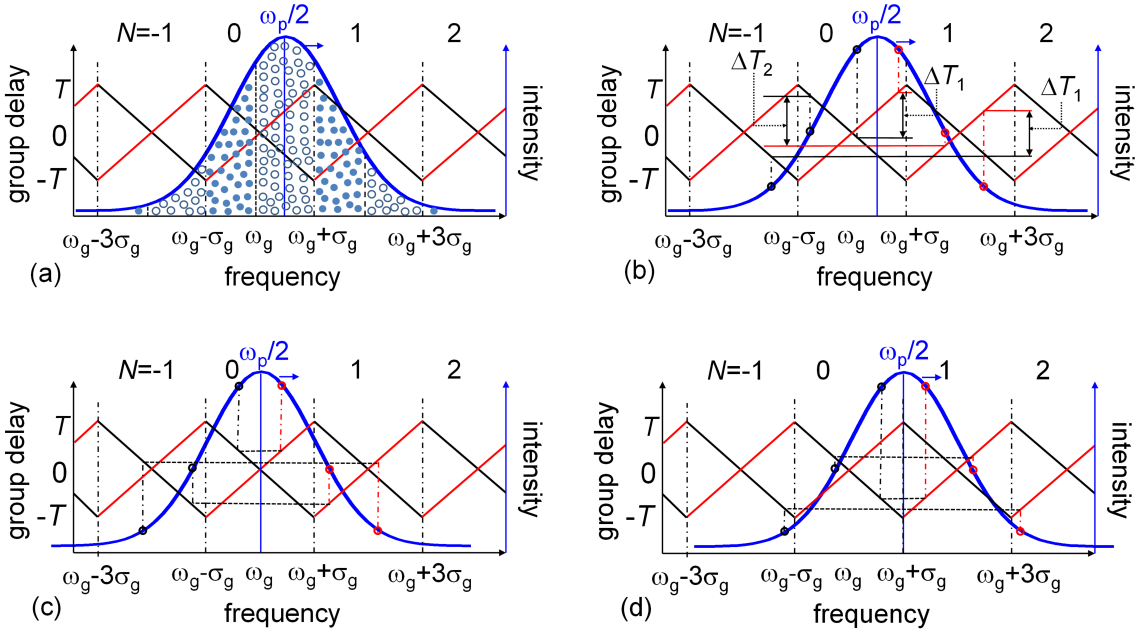

FIG. 4. (Color online)A graphic explanation of the double envelopes at general detunings ($\delta \neq 0$ and $\delta \neq \sigma_g$) and the single peaks at special detunings ($\delta = 0$ and $\delta = \sigma_g$). (a) At a general detuning ($\delta \neq 0$ and $\delta \neq \sigma_g$), the signal and idler photons experience different group delays resulting from the dispersive components. The group-delay differences have only two values: for the biphotons falling into the spectral region filled with open and filled circles, the group-delay differences are ΔT_1 and ΔT_2, respectively, as shown in (b). These two group-delay differences correspond to two envelopes in the coincidence histogram. (c) At the detuning of $\delta = 0$, the signal photon and its twin idler photon always experience the same group delay, corresponding to one peak at $\tau = 0$ in the coincidence histogram. (d) At the detuning of $\delta = \sigma_g$, the signal photon and its twin idler photon always experience the same group delay, corresponding to one peak at $\tau = 0$ in the coincidence histogram.

coincidence envelopes. At special detunings, $\delta = 0$ or $\delta = \sigma_g$, as shown in Fig. 4(c) and (d), respectively, signal and idler photons always experience the same group delay resulting from the dispersive components. Therefore, in these cases that the center of the biphoton spectrum is aligned with the centers or the edges of the channels, only one coincidence peak appears at $\tau = 0$. Complete cancellation of dispersion occurs, as shown in Fig. 3 (a) and (e).

V. CONCLUSION

We have investigated the temporal correlation of time-energy entangled photon pairs propagating through multi-frequency-channel dispersive components. Our investigations and results, in particular the unique features in coincidence histogram, would impact quantum metrology and communication. Because the total coincidences included in each envelope and the timing of each envelope are both sensitive to the detuning, as shown in Fig. 3 (i) and (j), either of them could be used for photon spectroscopy and Doppler velocimetry. Even narrower channel widths, $2\sigma_g$, are technically feasible; therefore, a tiny wavelength shift, δ, of the biphoton can be sensed. This effect can also be used in quantum communication to detect eavesdropping that may result in spectral changes of the photon pairs. In DWDM QKD systems, when photon pairs are tuned at the center or edges of a channel of the dispersive components, their correlations can be fully recovered through multi-frequency-channel dispersive propagation.

ACKNOWLEDGMENTS

The experimental work and the first phase of the theoretical work were supported by the DARPA Information in a Photon program, through grant W911NF-10-1-0416 from the Army Research Office. X. H. would like to thank Peiyang Scholarship from Tianjin University for supporting the second phase of the theoretical work. The authors would like to thank Alessandro Restelli and Joshua C. Bienfang for providing the self-differecing SPADs and relevant technical support, Jacob Mower and Catherine Lee for commenting on the manuscript.

[1] J. D. Franson, Phys. Rev. A **45**, 3126 (1992).
[2] S.-Y. Baek, Y.-W. Cho, and Y.-H. Kim, Opt. Exp. **17**, 19241 (2009).
[3] T. Zhong, and F. N. C. Wong, Phys. Rev. A **88**, 020103(R) (2013).
[4] A. M. Steinberg, P. G. Kwiat, and R. Y. Chiao, Phys. Rev. Lett. **68**, 2421 (1992).
[5] O. Minaeva, C. Bonato, B. E. A. Saleh, D. S. Simon, and A. V. Sergienko, Phys. Rev. Lett. **102**, 100504 (2009).
[6] K. A. O'Donnell, Phys. Rev. Lett. **106**, 063601 (2011).
[7] J. Mower, Z. Zhang, P. Desjardins, C. Lee, J. H. Shapiro, D. Englund, Phys. Rev. A. **87**, 062322 (2013).
[8] V. Giovannetti, S. Lloyd, L. Maccone, and F. N. C. Wong, Phys. Rev. Lett. **87**, 117902 (2001).
[9] M. B. Nasr, B. E. A. Saleh, A. V. Sergienko, and M. C. Teich, Phys. Rev. Lett. **91**, 083601 (2003).
[10] J. Mower, F. N. C. Wong, J. H. Shapiro, and D. Englund, arXiv:1110.4867 (2011).
[11] I. Ali-Khan, C. J. Broadbent, and J. C. Howell, Phys. Rev. Lett. **98**, 060503 (2007).
[12] From datasheets provided by Teraxion.
[13] T. Zhong, F. N. C. Wong, A. Restelli, J. C. Bienfang, Opt. Exp. **20**, 26868 (2012).
[14] X. Hu, T. Zhong, J. E. White, E. A. Dauler, F. Najafi, C. H. Herder, F. N. C. Wong, and K. K. Berggren, Opt. Lett. **34**, 3607 (2009).
[15] E. A. Dauler, A. J. Kerman, B. S. Robinson, J. K. W. Yang, B. Voronov, G. Gol'tsman, S. A. Hamilton, and K. K. Berggren, J. of Mod. Opt. **56**, 364 (2008).